Amino-Functionalized Monolithic Spin-Type Columns for High Throughput Lectin Affinity Chromatography of Glycoproteins

Senta Reichelt[a*], Christian Elsner[a], Andrea Prager[a], Sergei Naumov[a], J. Kuballa[b] and Michael R. Buchmeiser[c, d*]

[a]*Leibniz-Institut für Oberflächenmodifizierung, Permoserstr. 15, D-04318 Leipzig, Germany*

[b]*Galab-Technologies GmbH, Max-Planck-Str. 1, 21502 Geesthacht, Germany*

[c]*Institut für Polymerchemie, Universität Stuttgart, Pfaffenwaldring 55, D-70550 Stuttgart, Germany*

[d]*Institut für Textilchemie und Chemiefasern (ITCF), Körschtalstraße 26, D-73770 Denkendorf, Germany*

Quantum chemical calculations

Experimental Part. density functional theory (DFT) calculations were carried out using Becke's three-parameter functional (B3)[1,2] in combination with the Lee, Yang and Parr (LYP) correlation functional.[3] The molecular geometries, energies and frequency analysis were calculated at the B3LYP/6-31G(d,p) level of the theory as implemented in Jaguar program, version 7.6. From the frequency analysis thermochemical parameters as the zero point energy (ZPE), entropy (S) and Gibbs free energy (ΔG) were obtained at 298 K. Additionally, the solvent effect of residual water was checked for geometries optimized in the gas phase at the same level of theory using Jaguar's dielectric continuum Poisson-Boltzmann solver (PBF), which fits the field produced by the solvent dielectric continuum to another set of point.[4] However, the reaction parameters ΔH and ΔG of the intramolecular rearrangement and bimolecular reactions calculated in water differ from those calculated in the gas phase only within 2 to 3.5 kcal mol^{-1}, respectively. Thus, the reaction parameters calculated in the gas phase can be used for the analysis of the possible reaction ways. Radicals and ions, which might be generated by the radiolysis of water, were not considered in these calculations. The results are presented in the Table S3, Supporting Information.

Results. Quantum chemical calculations, based on simplified polymeric model (M) structures (M-PEG_ML, M-PAAm) consisting of two repeat units (Figure S6, Supporting Information) were performed to analyze the reaction mechanism between the PEG-based monolith (M-PEG_ML) and the grafting reagent PAAm. The influence of hydroxyl radicals, generated by the radiolysis of water, on the proceeding process was not considered in the calculation. First, the reaction species, which could contribute to the grafting reaction, were studied quantum chemically. During EB-treatment, primary radical cations are generated at the polymeric backbone. These can undergo either intramolecular rearrangement through H-shift (formation of a more stable secondary radical cation) or bimolecular (intermolecular) transformation through H-abstraction (formation of both a cation and radicals).[5,6] The most probable reaction mechanism for the reaction of PAAm with the PEG-monolith proceeds in two steps and is outlined in Figure S7, Supporting Information. The first step, i.e. the transformation of the primary radical cation M-PEG_ML($1^{\cdot+}$) into a secondary M-PEG_ML($2^{\cdot+}$) radical cation through an H-shift is strongly exothermic and exergonic. The radical cation then reacts with M-PAAm in its ground state through addition reaction, this reaction is nearly energy neutral. The overall reaction, however, is exothermic/exergonic and thus energetically favorable.

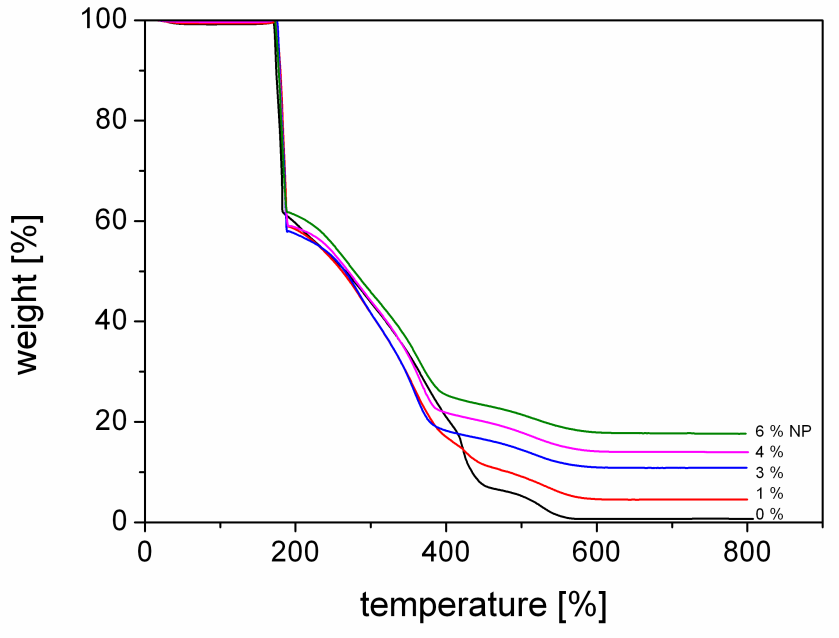

Figure S1: Thermogravimetric curve of monoliths type **A (0 wt.-% of nanoparticles)** and type **B** (1, 3, 4 and 6 wt.-% of nanoparticles, weight loss below T = 100 °C caused by the evaporation of water).

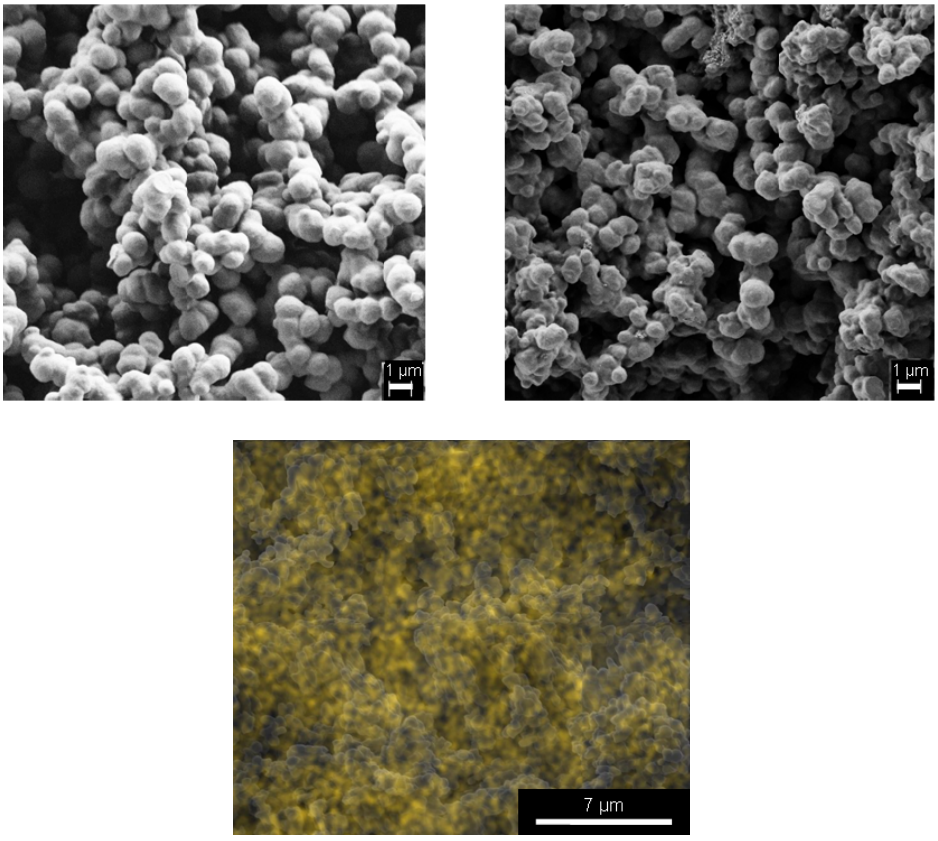

Figure S2. Scanning electron micrographs of monolith type **A** (left image), monolith type **B** (right image) and EDX-mapping of the silicon distribution of monolith type **B** (lower image).

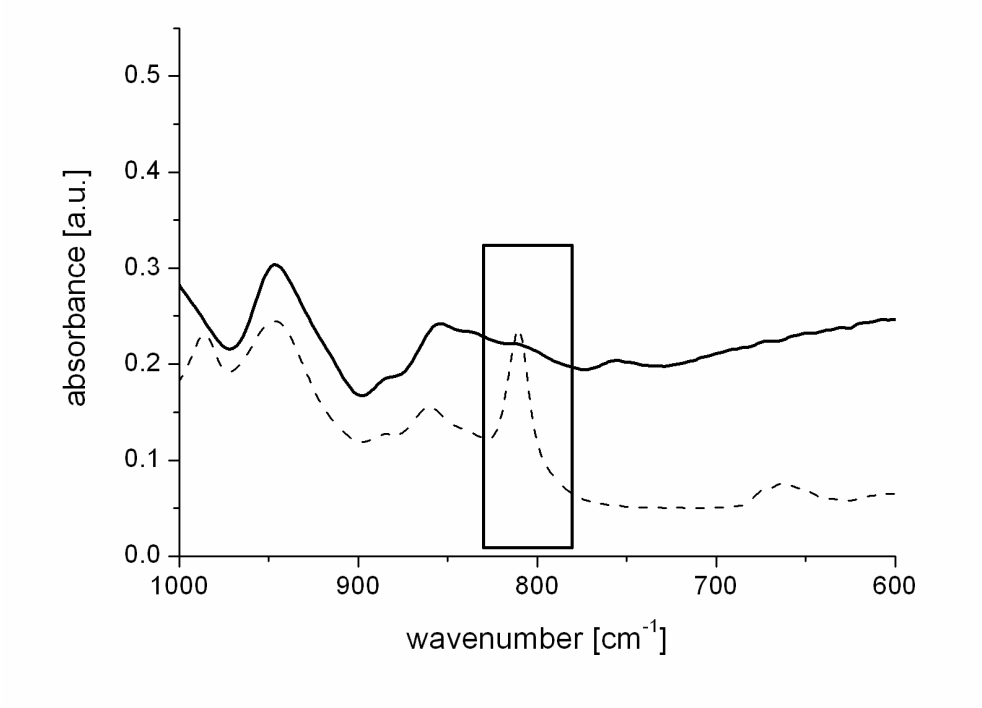

Figure S3: IR-spectroscopic determination of the double-bond conversion of the liquid formulation (dashed line) and in monolith type **B** (after washing and drying, solid line).

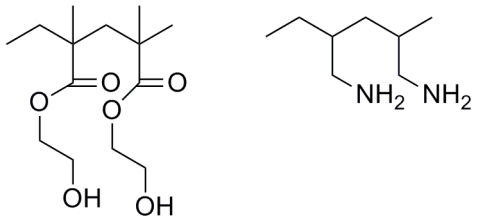

M-PEG_ML M-PAAm

Figure S4. Model structures of the polymers (M-PAAm) and the PEG based monoliths (M-PEG_ML) used for the computational study of the possible reaction pathways.

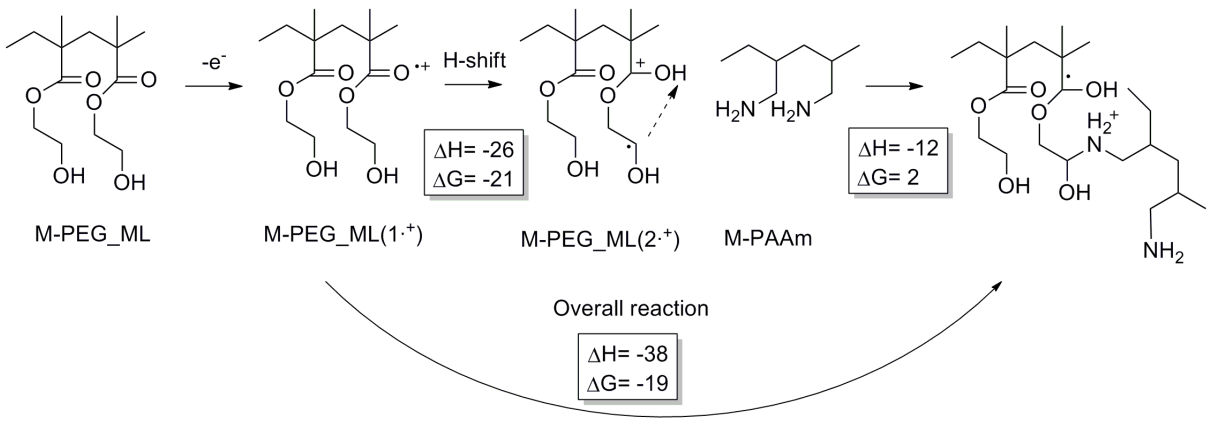

Figure S5. Most probable reaction pathway for the immobilization of PAAm based on the analysis of model systems. Reaction enthalpy (ΔH) and Gibbs free energy (ΔG) of reactions are given in kcal mol^{-1}.

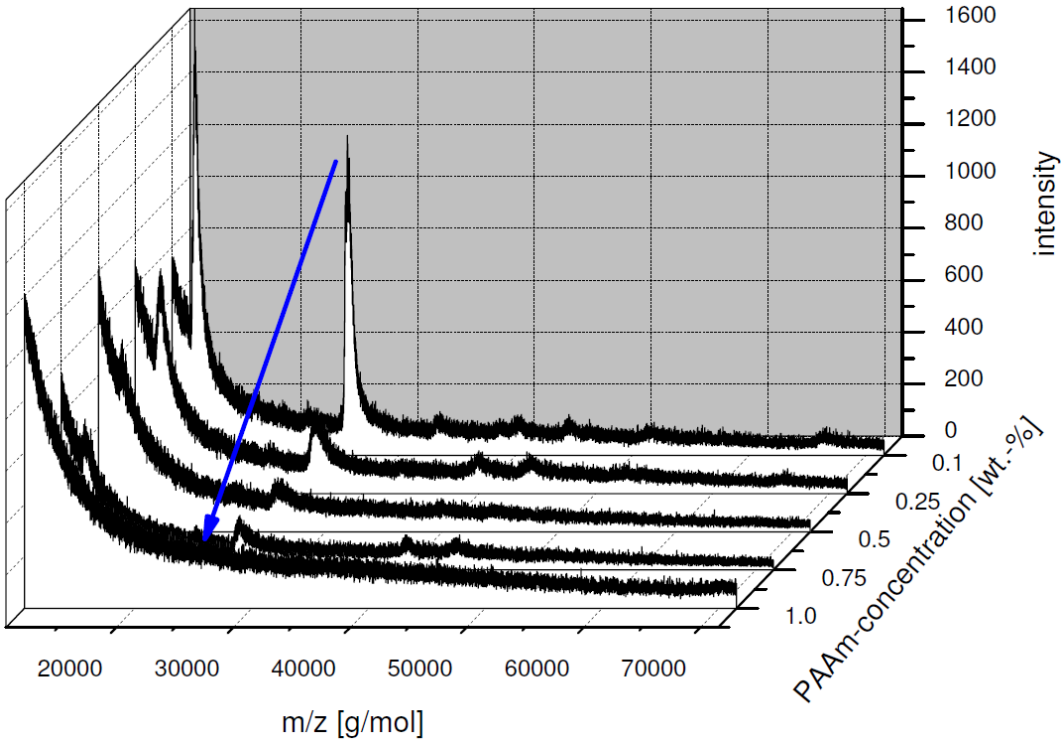

Figure S6. Decrease of the Con A peak in the washing fraction (F2) of PAAm-modified monoliths in dependence on the PAAm concentration.

Table S1. Influence of the weight-fraction of incorporated Ox50-particles on the median pore size of the resulting monoliths.

nanoparticle content [wt.- %]	**d_{50} [µm]**
0	9.4 ± 0.9
1	10.7 ± 1.77
3	12.0 ± 0.1
4	14.3 ± 0.7

Table S2. Influence of the PAAm concentration for surface-grafting on the average pore size of the resulting type **B** monoliths (3 wt.-% of Ox50).

C_{PAAm} [wt.-%]	**d_{50} [µm]**
0	12.0 ± 0.11
0.5	10.7 ± 0.6
1	8.8 ± 0.6
1.5	8.0 ± 0.4
2	8.3 ± 0.6

Table S3. Reaction enthalpy (ΔH) and Gibbs free energy (ΔG) of evaluated reactions of model systems in the gas phase.

	ΔH [kcal mol^{-1}]	ΔG [kcal mol^{-1}]
M-PEG_ML($1^{\cdot+}$)→M-PEG_ML($2^{\cdot+}$)	-26	-21
M-PEG_ML+M-PAAm$^{\bullet}$	34	19
M-PEG_ML+M-PAAm$^{\bullet+}$	0	15
M-PEG_ML($2^{\cdot+}$)+M-PAAm	-12	2
M-EMA_ML($1^{\cdot+}$)→M-EMA_ML($2^{\cdot+}$)	-1	2
M-EMA_ML($2^{\cdot+}$)+M-PAAm	-6	7

References

1. Becke, A. D., J. Chem. Phys., 98, 1993, 5648.
2. Becke, A. D., J. Chem. Phys., 104, 1996, 1040.
3. Lee, C. T.; Yang, W. T.; Parr, R. G., Phys. Rev. B, 37, 1988, 785.
4. Tannor, D. J.; Marten, B.; Murphy, R.; Friesner, R. A.; Sitkoff, D.; Nicholls, A.; Ringnalda, M.; Goddard, W. A.; Honig, B., J. Am. Chem. Soc., 116, 1994, 11875.
5. Janovsky, I.; Knolle, W.; Naumov, S.; Williams, F., Chem. Eur. J., 10, 2004, 5524.
6. Knolle, W.; Feldman, V. I.; Janovský, I.; Naumov, S.; Mehnert, R.; Langguth, H.; Sukhov, F. F.; Orlov, A. Y., J. Chem. Soc.-Perkin Trans. 2, 2002, 687.